Friction

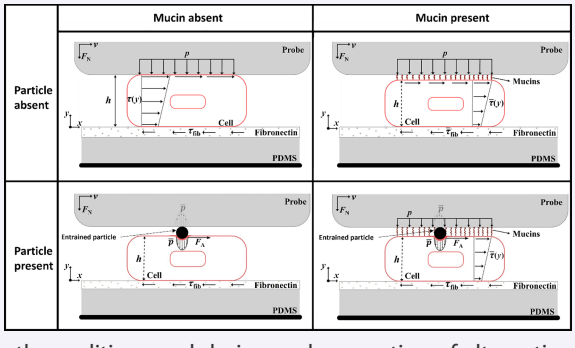
Research Article

Interface-level mechanisms of plant protein particles on friction and damage in in vitro biofidelic epithelial models

Samuel S. Gamaniel[1,2,✉], Ahranee Canden-Eastwood[2], Sam Davison[2], Rob Vreeker[3], David T. A. Matthews[1,4], Matt J. Carré[2], Roger Lewis[2], Emile van der Heide[1]

Cite this article: Gamaniel SS, Canden-Eastwood A, Davison S, et al. *Friction* 2026, **14**(11): 9441270. https://doi.org/10.26599/FRICT.2026.9441270

ABSTRACT: Epithelial surfaces rely on a mucous layer at contact interfaces to protect against mechanical stresses. Disruption of mucous lubrication compromises its protective function, increasing the exposure and vulnerability of underlying tissues to frictional damage. This study uses a novel biofidelic epithelial model that incorporates living cells, to study the interface-level mechanisms of friction, stress-induced cell membrane rupture and cell detachment in the presence and absence of mucous lubrication. This comprehensive approach bridges the disciplines of cell biology and tribology, offering new insights into particle-mediated lubrication at biological interfaces. This is relevant to understanding the heightened ocular and oral sensations associated with mucous lubrication failure, as seen in dry eye and dry mouth conditions and during oral perception of alternative plant protein ingredients such as fava bean protein isolate (FBPI). Friction experiments and subsequent cell damage analysis revealed that FBPI particles reduced friction by mitigating adhesion forces, while mucous layers further diminish shear-induced damage. In the absence of a mucous layer, stronger adhesive interactions at the cell-probe interface led to increased friction and cellular damage. Cell membrane rupture occurred when mechanical stresses exceeded critical thresholds, whereas detachment resulted from the breaking of fibronectin bonds at cell-fibronectin junctions. These findings highlight interface level mechanisms that can be applied towards the development of alternative food proteins and the further design of biofidelic testbeds.



KEYWORDS: mucous lubrication; plant protein particles; oral tribology; epithelial cells; friction

1 Introduction

Epithelial surfaces play a pivotal role as biological interfaces between the body and its environment, facilitating essential physiological functions. From a biomechanical perspective, these surfaces are exposed to complex mechanical interactions, including friction, adhesion, and deformation, under varying loads. Such interactions are particularly relevant in functionalities involving high stresses or repetitive contact, such as with biomedical devices, implants or when eating food. A protective layer of mucous proteins serves as nature's lubricant, shielding the epithelial cells from extreme shear forces. However, this mucous layer is susceptible to failure and leads to exposure of the epithelial tissues, rendering them vulnerable to mechanical stresses [1–3]. Understanding the mechanisms that lead to epithelial tissue exposure and cell damage is essential for unravelling the relationship between mechanical loads and cellular responses in a bio-tribological context [4].

Previous studies have examined the failure of boundary lubricating layers in machine elements which leads to local or gross lubrication losses and exposes underlying surfaces to direct contact between tribo-pairs [5, 6]. The presence of particles in such systems have also been identified as a significant cause of failure (wear) through mechanisms such as abrasion [7]. Similarly, in contacts involving biological tissues, particle-induced failure occurs. In extreme cases, these can lead to heightened sensations and/or mechanical micro-trauma on epithelial tissues. For example, protein particles interacting with biomimetic surfaces are a critical component of food research, as they influence texture and mouth feel by interacting with oral components, particularly through tribological and rheological phenomena [8–10]. Research shows how particles induce friction during sliding contacts with soft surfaces, exposing the role of adhesion, abrasion, lubrication disruption, and stress concentration [11, 12]. These interactions are highly dependent on specific systems and applications,

[1] Department of Mechanics of Solids, Surfaces, and Systems, Faculty of Engineering Technology, University of Twente, Enschede 7522 LW, the Netherlands. [2] School of Mechanical, Aerospace and Civil Engineering, University of Sheffield, Sheffield S1 3JD, UK. [3] Cosun RD & I, Cosun Innovation Center, Kreekweg 1, Dinteloord 4671 VA, the Netherlands. [4] Department of Materials Science and Engineering, Feng Chia University, Taichung City 407102, Taiwan, China.

✉ Corresponding author. E-mail: s.s.gamaniel@utwente.nl

Received: December 12, 2025; Revised: April 17, 2026; Accepted: May 22, 2026

© The Author(s) 2026. This is an open access article under the terms of the Creative Commons Attribution 4.0 International License (CC BY 4.0, http://creativecommons.org/licenses/by/4.0/).

highlighting the need for a more representative system to study the dynamic interplay between soft surfaces, particles and epithelial cells. Such a system becomes particularly important in scenarios where boundary lubricating layers fail to protect the epithelial layer from interactions that push the operating conditions beyond the physiological thresholds or limits typically tolerated by the tissue surface.

Recent advances in biotribology have driven the development of biomimetic platforms that progressively replicate key attributes of epithelial surfaces. Earlier models relied on untreated, simplified surfaces such as steel, glass, or smooth PDMS [2, 13, 14]. More recently, biomimetic textures that simulate the topology, wettability, and stiffness of the human tongue have been employed in tribological studies [15]. The most recent refinements include the adsorption of mucous boundary layers on soft surfaces to study boundary lubrication [5, 16]. These platforms have led to key findings based on the capabilities of the systems used in the corresponding investigations, including friction modulation, particle entrainment, boundary layer failure, and surface exposure [17–19].

What is missing, however, is an approach capable of representing the intricate dynamics of soft surfaces in contact with cells at these micro- and nano-scale interfaces, explaining the differences in failure mechanisms during typical applications such as the presence/absence of a protective mucous layer or the failure mechanisms resulting from the entrainment of plant protein particles.

The current work introduces a biofidelic epithelial model created by adsorbing mucous boundary layers onto an epithelial cell monolayer attached to PDMS. This innovative approach integrates friction testing with damage analysis of cell monolayers, to investigate the lubricating properties of plant protein particles. This is achieved by examining the interplay between particle-mediated lubrication, mechanical stresses, and cellular responses during the sliding contact of a PDMS probe on a cell monolayer. The aim of this study is to uncover how the presence or absence of protein particles or a lubricating mucous layer influences the interaction mechanisms at the oral contact interface. With this study, a link between contact mechanisms, friction signals, number of dead/detached cells, and cell monolayer damage patterns is established, providing a unique perspective to understanding how stresses are transferred to the underlying tissues during sliding contact.

2 Materials and methods

2.1 Materials

Silicone elastomer Sylgard 184 purchased from Dow Silicones Corp., USA, was used in preparing the PDMS probes whereas substrates were prepared using soft PDMS GEL-8100 purchased from NuSil Technology LLC, USA. Phosphate buffered saline (PBS) powder purchased from Sigma Aldrich, USA, was used as a buffer solution throughout this work. Bovine submaxillary mucins (BSM) type I-S purchased from Sigma Aldrich, USA, was used as a model for salivary mucous proteins. Fava bean protein isolate (FBPI) was provided by COSUN (Dinteloord, the Netherlands). Fibronectin from bovine plasma was purchased from Gibco (33010-018). Cell culture medium was prepared from Iscove's Dulbecco's Modified Eagle's Medium (Iscove's DMEM) purchased from Corning Inc., USA, 1% penicillin-streptomycin, and 10% fetal bovine serum. The cell line used was an immortalized human oral squamous carcinoma cell line, PE/CA-PJ15 (catalogue number 96121230) which was purchased from Culture Collections, UK. PE/CA PJ15 cells were chosen because they provide reproducible, mechanically consistent monolayers ideal for controlled tribological testing, enabling clear comparison of interaction mechanisms even if absolute damage thresholds may differ from native oral tissues.

2.2 Methods

2.2.1 Preparation of mucin solution and fava bean protein isolate dispersion

BSM solution was prepared by dissolving BSM in PBS at a concentration of 3.0 wt% for 8 h. To obtain a purified BSM solution, dissolution was followed by protein dialysis using a Spectra-Por dialysis column (100 kDa MWCO) against PBS for 48 h. The purified BSM solution was stored between 2 and 8 °C. FBPI colloidal dispersions in PBS was prepared following the procedure described in Ref. [5].

2.2.2 Probe and substrate fabrication

The PDMS substrates were prepared by mixing NuSiL PDMS pre-polymer part A and part B in a 1:1 ratio and adding 1 wt% of curing agent before stirring for at least 2 min. The mix was placed in vacuum to evacuate trapped air before pouring 2 g into each tissue culture plate. Samples were returned to the vacuum to evacuate any newly introduced air before incubating overnight at 70 °C. The final substrate had a diameter ϕ = 35 mm and Young's modulus E_1 = 73.32±2.96 kPa [2].

A hemispherical PDMS probe was chosen for these experiments because it provides a well-defined and reproducible contact geometry with uniform pressure distribution, enabling the application of the Hertzian contact theory while maintaining biocompatibility under physiologically relevant conditions. PDMS probes were prepared by mixing Sylgard 184 pre-polymer with a curing agent in a 10:1 mix ratio and stirring for at least 2 min. Air bubbles in the mix were evacuated by placing in vacuum before gently pouring the uncured polymer into a 96 microwell mold (Greiner bio-one, Germany). The uncured polymer was placed in vacuum once more before curing in the oven at 60 °C for 3 h. The resulting PDMS probes had hemispherical tips of R = 3 mm, Young's modulus E_2 = 2.4 MPa, and a centre line average roughness Ra = 2.69 μm. The probe holder was printed using a masked stereolithography apparatus (MSLA Original Prusa SL1S).

2.2.3 Tissue culture plate preparation

Tissue culture plates were prepared following the procedure described previously in Ref. [2]. Briefly, PDMS substrates were washed thoroughly with 70% industrial methylated spirit (IMS) and washed 3 times with 3 mL PBS. 2 μg·cm^{-2} of fibronectin solution was prepared, and 3.5 mL of the solution was adsorbed onto each tissue culture dish before incubating at room temperature for 24 h. A human oral squamous carcinoma cell line (PE/CA-PJ15) was cultured in Iscove's DMEM and grown until at least 70% confluent at 37 °C, 95% relative humidity, and 5% CO_2. Cell suspension was collected and centrifuged at 500g (relative centrifugal force, r.c.f) for 5 min. Upon removing the supernatant, cells were resuspended in 3 mL of cell culture media until a seeding density of 20,000 cells/cm^2 was achieved. Tissue culture plates with adsorbed fibronectin were washed 3 times with PBS prior to cell seeding. These were then incubated at 37 °C, 95% relative humidity, and 5% CO_2 until they reached 85%–90% confluency and were determined ready for testing.

2.2.4 Sliding friction tests

A universal mechanical tester (UMT) tribometer (Bruker, USA)

was used in a pin-on-plate configuration to apply constant loading and sliding conditions while measuring the friction forces. Each test was conducted by sliding a PDMS probe across a distance d = 10 mm at a velocity v = 1 mm/s, applying a constant normal load F_N = 20 mN. The friction force was recorded throughout the test to calculate the coefficient of friction (COF). Figure 1 illustrates a typical representation of the friction force, normal force, and COF signals. The resulting Hertzian contact pressure can be calculated as

$$p_H = \frac{3F_N}{2\pi a_H{}^2} \quad (1)$$

where the Hertzian contact area a_H is given by

$$a_H = \left(\frac{3F_N R}{4E_e}\right)^{\frac{1}{3}} \quad (2)$$

The equivalent Young's modulus E_e is calculated as

$$E_e = \frac{E_1 E_2}{E_2(1-\nu_1{}^2) + E_1(1-\nu_2{}^2)} \quad (3)$$

where the Poisson ratio of PDMS is taken as ν = 0.49. The calculated Hertzian contact pressure p_H = 15.7 kPa, falls within the estimated range of compressive pressures (2–70 kPa) exerted on epithelial tissues during tongue interactions with other oral surfaces [20, 21]. Four different lubricating conditions were tested using PDMS probes on the cell monolayer in tissue culture plates: (i) particles and mucous lubrication absent via a control test case where the cell monolayer was exposed with no proteins present (only PBS) on the surface, (ii) particles present in the contact via a 0.5 wt% FBPI dispersion only, (iii) mucous lubrication (ML) present via a BSM layer only, and (iv) particles and mucous lubrication present via a 0.5 wt% FBPI dispersion on BSM boundary layer (FBPI-ML). The FBPI concentration was chosen because it provides a well-dispersed system for studying particles effects. Higher concentrations can lead to a dense FBPI layer where shear occurs within the layer rather than at the probe–cell interface [22]. The BSM boundary layer was formed by adsorbing 3 mL of 3.0 wt% of BSM solution onto the cell monolayer surface for 5 min before washing with PBS. All tests were repeated 6 times and used 1 mL of either FBPI dispersions or PBS solutions in the tissue culture plates. Following each sliding friction test, the PBS/FBPI was aspirated from the tissue culture plate, and the cell monolayer was washed with PBS to ensure removal of cells detached during the sliding contact.

2.2.5 Live/dead imaging assay

Following each sliding test, 1 mL of the staining solution was poured into the tissue culture plate and incubated for 15 min at 37 °C and 5% CO_2. A cell staining solution was prepared using 0.15 mg/mL propidium iodide (PI) and 5 μg/mL Hoechst 33342, trihydrochloride trihydrate in PBS. PI was used to detect the dead cells and Hoechst solution was used as a counterstain for the live cells. The stained cell monolayer was afterwards rinsed with 2 mL of PBS and 1 mL of cell medium was added to the sample in preparation for imaging.

The cell monolayer was imaged using a Nikon Eclipse Ti fluorescence microscope (Nikon Instruments, Japan). Dead cells stained with PI were visible at an excitation wavelength of 488 nm and an emission wavelength of 617 nm, whereas live cells stained with Hoechst solution were visible at an excitation wavelength of 361 nm and emission wavelength of 486 nm.

Images obtained from the fluorescent microscope were post processed using ImageJ software (version 2.14.0, USA) [23, 24]. Cell counts for both live and dead cells were done using the Cell Counter plugin (version 3.0.0) whereas the Image J built-in measurement function was used to calculate the relative fluorescent intensities.

2.2.6 Statistics

Significant differences between the COF and live-dead cell counts were determined by one-way ANOVA using the Kruskal–Wallis test [25]. p-values were also obtained via post-hoc pairwise comparisons using Dunn's test with Bonferroni adjustment. Statistical analyses were done in Python (version 3.10.11) using the *scipy* library [26] and *scikit-posthocs* package [27]. Tests were considered statistically significant when the p-value for significance was below the 0.05 threshold.

2.2.7 Damage assessment

A typical image from a sliding test after the live–dead imaging assay described in Section 2.2.5 is presented in Fig. 2 annotated

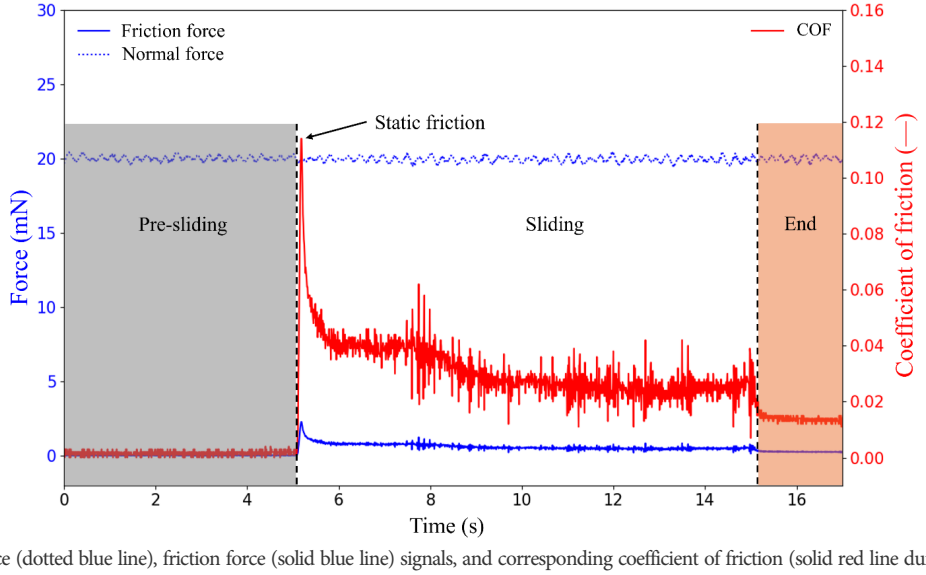


Fig. 1 Raw normal force (dotted blue line), friction force (solid blue line) signals, and corresponding coefficient of friction (solid red line during sliding) for a typical sliding test showing the signals before sliding, at the onset of sliding, during, and after sliding. In the pre-sliding (shaded grey) and end (shaded orange) zones, the solid red line represents the ratio of the friction and normal forces.

with a slide region and two control regions. In these images, the red spots indicate the dead cells, the blue spots indicate the live cells, and the dark grey background correspond either to areas lacking cell coverage or locations where cells were detached during sliding.

After cell counting, the number of detached cells (Δ_s) was estimated by subtracting the number of cells remaining in the slide region from the number of cells that were initially present in the slide region, assuming that the average cell densities for both control and slide regions were equal before sliding, such that

$$\Delta_s = A_{sc} \cdot (L_c + D_c) - (L_s + D_s) \tag{4}$$

where A_{sc} represents the ratio of the sliding contact area to the control region area, L is the counted number of live cells, D is the counted number of dead cells, and the subscripts c and s denote whether the cells were counted in the control or sliding regions, respectively. As the cell numbers can vary between the tissue culture plates, cell counts are reported as a fraction of the total number of cells for each tissue culture plate.

3 Cell damage mechanisms

When cells are adhered to a substrate, their deformation and damage are largely dependent on the interactions with the environment. Techniques to investigate the mechanical and failure properties of cells such as their stiffness, surface tension, hydrostatic pressure, rupture loads, and the shear stresses necessary for detachment are available from Refs. [28–30]. These properties are directly related to how cells react under different mechanical loads, outlining the critical values beyond which damage may occur to cells adhered to a substrate.

In the context of this study, damage can be categorized as either cell death or cell detachment. Cell death may be caused by probe-induced cell wall rupture or by particle-induced cell wall rupture. Cell detachment occurs when the probe, during sliding, removes cells that were previously adhered to the PDMS substrate. This section presents a hypothesis regarding the possible mechanisms of cell damage (death and detachment) during probe–particle–cell interactions, as well as the potential role of mucous lubrication at the interface, which will be tested through subsequent experiments and analysis. To make this assessment, four possible interaction modes are considered, combining when mucous lubrication is present or absent with when a particle is present or absent at the probe–cell interface. Figure 3 illustrates the four different interaction modes for a system entirely submerged in a PBS buffer to maintain physiological conditions. Two assumptions are made

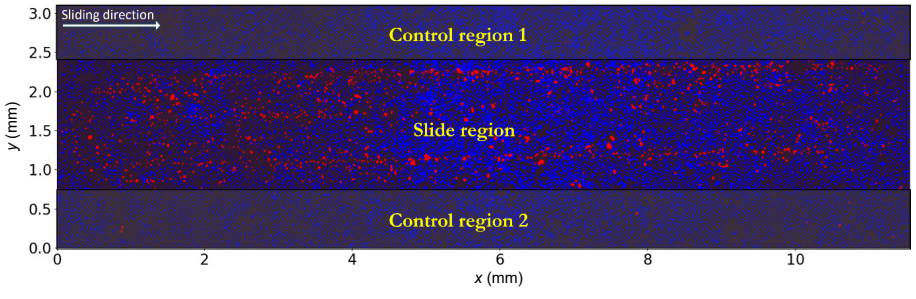


Fig. 2 Live–dead cell assay of the cell monolayer, highlighting the sliding direction, slide region, and control regions used to calculate live (blue), dead (red), and removed cells.

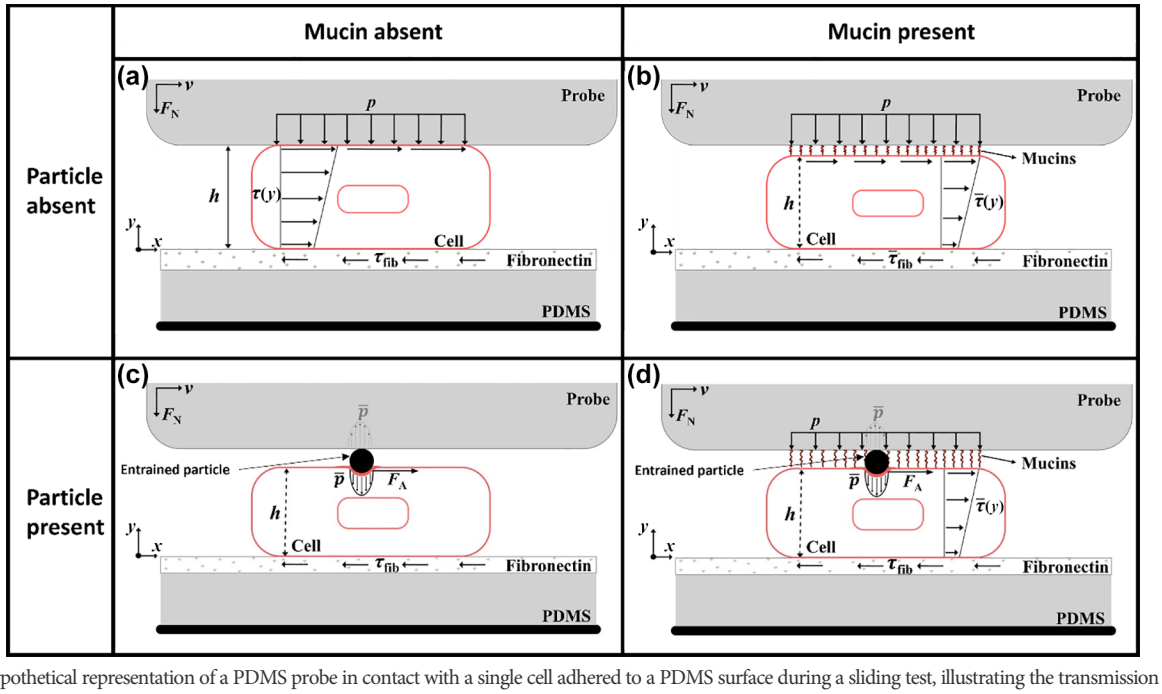


Fig. 3 Hypothetical representation of a PDMS probe in contact with a single cell adhered to a PDMS surface during a sliding test, illustrating the transmission of forces responsible for friction, localized cell pressure, and cell damage. Forces are transmitted from the probe to the cell and the underlying fibronectin layer when (a) mucous lubrication and particles are absent (only PBS), (b) only mucous lubrication present, (c) only entrained FBPI particles present, and (d) entrained FBPI particles and mucous lubrication present at the cell–probe interface. The entire system is submerged in PBS to maintain physiological conditions.

with respect to the contacting surfaces: (i) The probe and cell contact geometry is axisymmetric, smooth, and continuous, i.e., perfectly aligned with no roughness at the cell–probe interface, and (ii) the cell width is much smaller than the contact radius such that the effect of the probe curvature can be neglected and it is taken as a flat on flat contact. In this section, the expected failure modes occurring during these interactions are examined.

3.1 Probe induced cell death by cell membrane rupture

A cell completely exposed and in direct contact with the sliding probe is subjected to both a constant normal load (F_N) and velocity (v), as shown in Fig. 3(a). F_N is transmitted over the contact area (A) in the form of a uniform pressure distribution p. The sliding action of the probe generates a friction force (F_f) which in this case is the sum of the force needed to supply energy of deformation ($F_{f,def}$) and the force to shear adhered junctions ($F_{f,adh}$) at the cell–probe interface:

$$F_f = F_{f,def} + F_{f,adh} \tag{5}$$

Following the assumption of a smooth, axisymmetric, and continuous contact while neglecting the effect of the probe curvature, the deformation term $F_{f,def}$ is considered to be zero. The adhesion term can be defined as

$$F_{f,adh} = \tau \cdot A \tag{6}$$

where τ is the shear stress. The exerted pressure and shear forces at the cell–probe interface can tear sections of the cell wall, depending on the limiting shear strength of the cell membrane. Considering the cell membrane to be a thin film that houses the cytoplasm with a uniform hydrostatic cell pressure exerted on the cell membrane, there exists a critical pressure p_{max} and a critical shear stress (membrane shear strength) τ_{max} such that when: (i) $p > p_{max}$ or (ii) $\tau(y) > \tau_{max}$, a resulting strain induced cell membrane rupture leads to cell death [31]. The shear stress at the cell–probe interface $\tau(h)$ is related to the contact pressure p by

$$\tau(h) = \mu p \tag{7}$$

where μ corresponds to the COF at the cell–probe interface. The critical mechanical thresholds for cell membrane rupture under different loading conditions are available from the literature, including Peeters et al. [32] who investigated the mechanical properties of adherent cells under compressive forces, determining critical rupture forces and threshold strain values beyond which cell failure occurred. Another study by Ludwig et al. [33] demonstrated the influence of shear stresses on cells adhered onto a surface, showing irreversible morphological changes and death at a determined critical shear stress. These studies highlight how cell membrane failure is governed by both stress magnitude and loading dynamics.

3.2 Probe induced cell detachment

Below the critical stresses required for probe-induced cell death by membrane rupture, a cell directly exposed to the probe (see Fig. 3(a)) is susceptible to detachment. During probe sliding, the shear stress at the cell–probe interface $\tau(h)$, is transmitted to the cell–fibronectin interface $\tau(0)$, thereby influencing the mechanical interactions at cellular adhesion points. Fibronectin coatings mimic the extracellular matrix (ECM) by forming adhesive joints (fibrils) that hold the cells fixed to the substrate. When exposed to shear, there exists a critical shear stress τ_{fib}, beyond which adhesive bonds break and cells detach from fibronectin-coated surfaces [30]. In such cases, cell detachment is expected to occur when $\tau(0) > \tau_{fib}$.

Dunn et al. [3] conducted friction tests to determine normal loads and shear stresses beyond which cell detachment forces were large enough to overcome the adhesive forces. Thoumine et al. [34] described this phenomenon of cell adhesion rupture for cells adhered to microplates via fibronectin and proposed a model to predict the critical forces required for detachment.

Within the sliding region, a cell in equilibrium can therefore be defined as one that satisfies the conditions $p \leqslant p_{max}$, $\tau(y) \leqslant \tau_{max}$, and $\tau(0) \leqslant \tau_{fib}$, ensuring that a cell in contact with the sliding probe stays alive and remains adhered to the surface after the experiment.

3.3 Mucous boundary lubrication

The presence of a mucous boundary layer on the cell monolayer as shown in Fig. 3(b) introduces a new interface that alters the previously described mechanical interactions at the cell–probe interface. The superior lubricating property of bovine submaxillary mucins is expected to reduce the friction coefficient from μ (when mucin is absent and the cells are fully exposed) to $\overline{\mu}$, as adhesive junctions are replaced by a hydrated protein layer. The shear stress at the cell–probe interface when a mucous layer is adsorbed, becomes

$$\overline{\tau}(h) = \overline{\mu} p \tag{8}$$

This indicates that the shear forces at both the cell–probe interface and the resulting shear stresses at the cell–fibronectin interface are reduced due to mucous boundary layer lubrication. Consequently, it becomes less likely that in the presence of a mucous lubricating layer cell death occurs from $\overline{\tau}(y)$ reaching the critical value $\overline{\tau}_{max}$, or for cell detachment to result from $\overline{\tau}(0)$ reaching the critical shear stress $\overline{\tau}_{fib}$.

3.4 Particle induced cell membrane rupture

A particle entrained into the contact at the cell–probe–interface as illustrated in Figs. 3(c) and 3(d) separates the contact between the probe and the cell. In the boundary lubrication regime, the presence of particles in the sliding contact, reduces the contact area, increases the contact pressure, and decreases the friction force compared to an exposed cell–probe contact [35, 36]. Particles with an average diameter less than the cell diameter will act as an indenter on the cell membrane, exerting a pressure $\overline{p}$ that is much greater than p (the pressure when the cell is in contact with the probe). The effect of a spherical probe exerting force on a cell has been studied using atomic force microscopy (AFM) and finite element modelling, demonstrating a rapid increase in stresses around the contact region that is sufficient to reach the failure strain for cell membrane rupture [37, 38]. Depending on factors including particle shape, size, hardness, substrate deformation, and film thickness, a particle within a contact may roll, slide, or become embedded in one surface while being dragged across the surface, causing a steep increase in both contact pressure and force of abrasion (F_A) at the point of contact with the particle.

Together, the interaction modes presented in this section form a testable hypothesis regarding the mechanisms of cell damage during probe–particle–cell interactions and the potential influence of mucous lubrication, which the experiments and analyses have been designed to evaluate.

4 Results

The results from this study showed that there were significant

differences across all experiments in the calculated COF ($H(3) = 13.23$, $p = 0.004$) and calculated damage ($H(3) = 9.55$, $p = 0.023$) to the cell monolayer.

The results in Fig. 4 show that the highest friction occurred when cells were completely exposed to the PDMS probe in the presence of a PBS buffer, which also resulted in the greatest damage (cell death and detachment) on the cell monolayer. The introduction of FBPI reduced the COF compared to a fully exposed cell monolayer due to the entrainment of protein particles in the contact; however, similar levels of cell damage were observed in both cases. The observed differences in COF and the similarities in cell damage in the presence and absence of FBPI particles suggest that the assumption of friction being directly related to cell damage may not be valid in this case. This means that there may be at least two distinct cell damage mechanisms occurring when the probe interacts with the cell monolayer under the conditions investigated.

Adding a mucous boundary layer to the cell monolayer reduced both friction ($p = 0.002$) and cell monolayer damage ($p = 0.133$) compared to when no mucous was present on the cell monolayer. The presence of FBPI on the mucous boundary layer resulted in a COF similar to what was observed when FBPI alone was present without the mucous layer, although slightly higher than when only the mucous layer was present. Cell monolayer damage in the presence of FBPI on the mucous layer was greater than when only the mucous layer was present ($p = 0.053$) and similar to the damage recorded when only FBPI was present on the cell monolayer. The low friction levels and higher damage recorded when FBPI was present compared to other experiments suggest that FBPI contributes to a cell damage mechanism that is independent of the shear stress, which was previously considered to be the major cause of cell damage [4, 39].

Analysing the mode of damage as either cell death or cell removal provides further insights into the underlying damage mechanisms. In Fig. 5, the cell monolayer damage data are split into two sub-sets, consisting of dead cells and detached cells. When the mucous layer was absent on the cell monolayer (PBS and FBPI), there was a higher amount of cell death and cell detachment compared to when a mucous layer was present with no FBPI. Adding FBPI to the mucous layer resulted in a significant increase in the number of cell deaths ($p = 0.009$). The level of cell detachment when FBPI particles were present on the mucous layer was similar to when only the mucous layer was present. The percentage of cell detachment when FBPI was present on a mucous layer was lower than both cases where there was no mucous layer.

Figure 6 provides fluorescent images with visual representation of the cell monolayer after sliding contact with the probe for the different cases investigated. The region of the probes' initial indentation is circled, and the slide path is highlighted, both in yellow. Figure 6(a) corresponds to a sliding test where only PBS was present on the cell monolayer and shows areas in the slide path containing live cells in blue, dead cells in red, and regions where cells have been detached, indicated by the empty (dark) regions along the sliding path. Figure 6(b) represents the cell monolayer after only FBPI was present during sliding. At the onset of sliding, a repetitive pattern of removed cells, matching the shape of the leading edge of the contact region of the sliding probe suggests that stick–slip had occurred. This observed stick–slip behavior results from alternate periods of sticking and slipping when transitioning from static to dynamic friction and has been studied in contacts involving soft surfaces [40, 41]. The sticking phase is characterized by increased friction forces, often resulting in a build-up of stress at the interface, which in turn causes the observed cell deaths and removal indicated by the red and dark annotated stick–slip pattern in Fig. 6(b). During slipping, the energy stored at the interface drives accelerated motion, accompanied by a rapid drop in the friction force that leads to local separation or sliding until stresses are redistributed. The combined action of sticking and slipping produced the annotated pattern shown in Fig. 6(b). Additionally, a continuous stretch of dead cells along the sliding path was observed, beginning at the region of indentation. A similar pattern of dead cells is visible in Fig. 6(c), when FBPI was present with a mucous layer. This effect which was visible in both experiments when FBPI was present with and without a mucous layer suggests that during initial probe indentation some FBPI particles were adhered onto the probe and were dragged along the cell monolayer causing abrasion. A typical characteristic of this abrasive wear mechanism is parallel lines/grooves on the abraded surfaces [42, 43].

5 Discussion

Results presented in this study indicated that the greatest amount of damage occurred when the cell monolayer was exposed to mechanical loads during contact with the sliding probe in the absence of mucins and particles at the cell probe interface. The cell damage data reported in Fig. 4 when the exposed cells were in contact with the probe can be attributed to either: (i) the contact pressure on individual cells being larger than the critical threshold for cell membrane rupture, or (ii) the shear stresses at the cell–probe interface exceeding the cell membrane shear strength (critical shear stress). Given the calculated Hertzian contact pressure ($p_H = 15.7$ kPa) and average calculated coefficient of

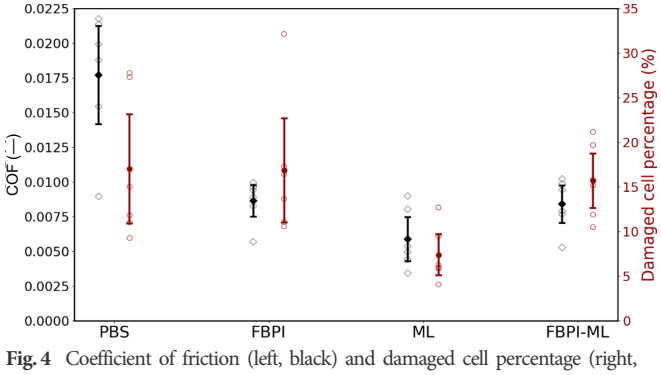


Fig. 4 Coefficient of friction (left, black) and damaged cell percentage (right, red) showing fractions of damaged cells (sum of dead and detached cell fractions) when PBS buffer, FBPI, mucous layer (ML), and FBPI on ML (FBPI-ML) were present on an epithelial cell monolayer during friction tests.

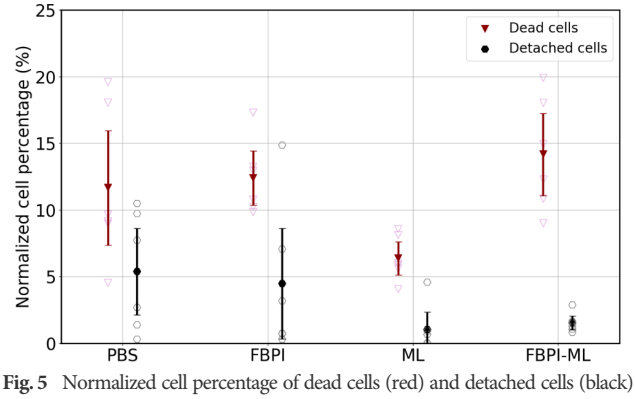


Fig. 5 Normalized cell percentage of dead cells (red) and detached cells (black) when PBS buffer, FBPI, mucous layer (ML), and FBPI on ML (FBPI-ML) were present on an epithelial cell monolayer during friction experiments.

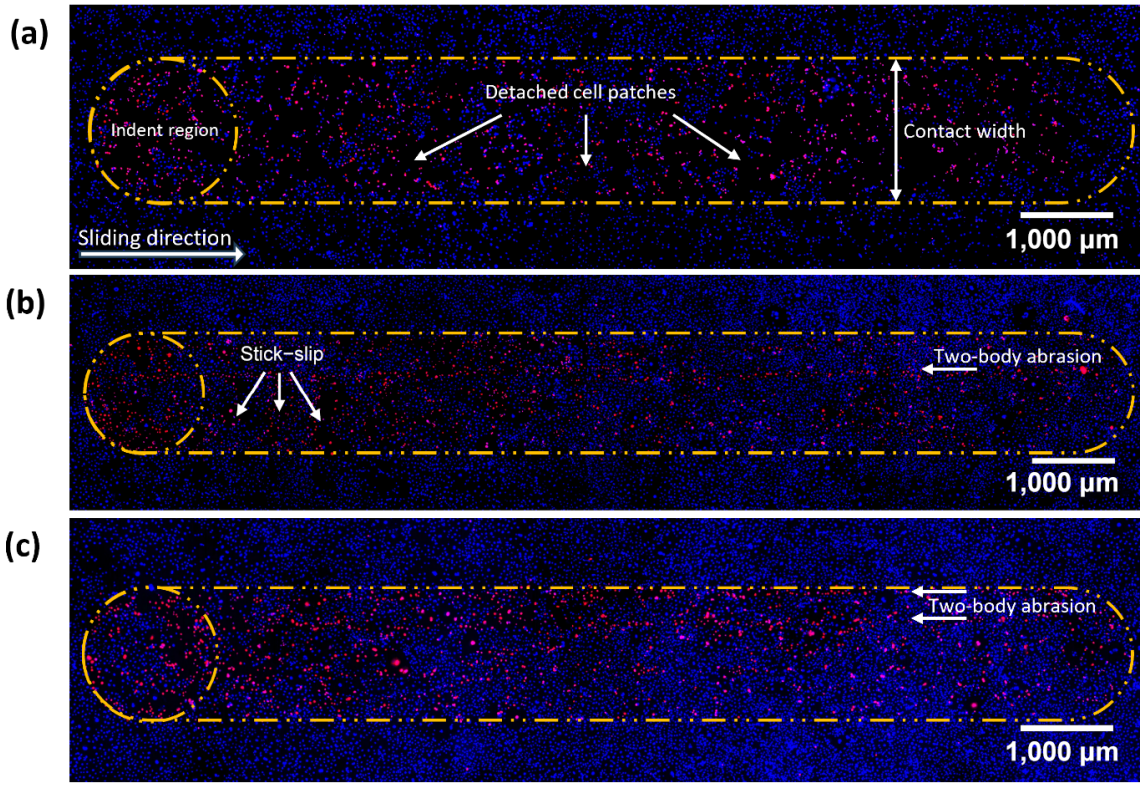


Fig. 6 Images of fluorescence labelled epithelial cell monolayer showing live cells (blue) and dead cells (red). Initial indentation region is circled, and contact region is highlighted, both in yellow. Images were obtained after sliding contact of the cell monolayer with a PDMS probe under lubricating conditions: (a) Particles and mucous lubrication absent such that cell monolayer was fully exposed, (b) particles present as FBPI dispersion with no mucous lubrication, and (c) particles and mucous lubrication present as FBPI dispersion present on an adsorbed mucous layer.

friction $\mu = 0.0175$, it is possible, using Eq. (7), to give an estimated value for the shear stress when the cells were exposed to the probe in the absence of mucins or particles as $\tau = 275$ Pa.

A lower occurrence of cell death and detachment was reported following tests where the mucous boundary layer was present on the cell monolayer compared to those where it was absent. This could be attributed to the lower average coefficient of friction $\overline{\mu} = 0.006$ resulting in a reduced average shear stress value $\overline{\tau} = 94$ Pa, as estimated using Eq. (8). This reduction in shear stresses is noticeable for experiments with a mucous layer as they resulted in the lowest amount of cell deaths and cell detachment, suggesting that the critical shear stresses of the cell membrane τ_{max} and cell-fibronectin adhesive junctions τ_{fib} were not exceeded. Despite the improved lubrication properties of the mucous layer, there were still cell deaths occurring, this is attributed to the unchanged pressure distribution exerted by the probe on the cell plausibly leading to pressure induced cell membrane rupture similar to what was observed in indentation tests by Ref. [44].

FBPI particles present at the cell–probe interface resulted in a lower coefficient of friction ($\overline{\mu} = 0.009$) compared to conditions where the cell monolayer had neither mucins nor FBPI present. In experiments involving FBPI present on a mucous layer, the coefficient of friction dropped further to $\overline{\mu} = 0.006$, similar to results observed when only mucins were present. Despite these differences in coefficient of friction when FBPI was tested in the presence or absence of a mucous layer, both conditions led to similar levels of cell damage. The observed differences in interfacial shear stress (proportional to the COF in this case) when FBPI was tested in the presence and absence of a mucous layer, coupled with the comparable levels of cell damage, suggests that the presence of FBPI at the cell–probe interface induces cell damage through mechanisms other than shear stress induced cell membrane rupture.

When FBPI was present on a mucous layer, the lowest number of cell detachments was observed (comparable to tests with only the mucous layer present), indicating that the critical shear stress τ_{fib} was not reached. However, this same experiment resulted in the highest number of cell deaths. Considering the properties of the interacting components, oral squamous epithelial cells typically have diameters ranging from 60 to 100 μm, while FBPI particles average 45 nm in size (see Appendix) [45]. Due to its smaller size, each particle at the contact interface acts as an indenter on the cell membrane, exerting a pressure $\overline{p}$ that is much greater than p_H. The reduction in contact area as a result of particles within the contact, together with the corresponding increase in contact pressure at localized probe–particle–cell regions, explains the observed decrease in friction levels and the corresponding rise in cell deaths during experiments involving FBPI particles. The results also indicated that the presence of the mucous boundary layer during experiments involving FBPI particles, did not significantly affect the coefficient of friction or the number of dead cells. This supports the hypothesis that the observed damage in the presence of particles was primarily due to pressures exceeding critical threshold values at the probe–particle–cell interface, rather than being entirely as a result of changes to the friction forces. This lubrication–protection dissociation implies that there may be limitations to oral tribological assessments using only the COF as metric for evaluating particulate systems.

6 Conclusions

This study investigated the lubricating properties of plant protein

particles on an in vitro biofidelic epithelial model, focusing on probe–particle–cell interaction mechanisms, and their correlation with friction and the extent of damage to the cell monolayer. While many concepts discussed in this work have been previously studied for soft surfaces in the absence or presence of particles, the novelty of this study lies in its ability to establish a link between friction behaviour, cell monolayer damage patterns, dead cell fractions, and detached cell fractions. The comprehensive approach of this research bridges the disciplines of cell biology and tribology, providing new insights into particle-mediated lubrication at biological interfaces. This made it possible to identify a dissociation between lubrication performance and cell-monolayer protection, indicating that the COF alone may not adequately represent the relevant oral interaction mechanisms in particulate systems. Other key findings from this study include:

(i) Compared to a cell monolayer fully exposed to a sliding probe, FBPI particles reduced the contact area, increased the local contact pressures at the particle–cell interface and decreased friction. The higher friction forces observed for fully exposed cell monolayers were primarily attributed to the forces required to break adhesive bonds formed at the cell–probe interface during sliding. In contrast, the presence of FBPI particles, an adsorbed mucous layer, or both significantly reduced the influence of adhesion forces, resulting in lower friction forces during sliding.

(ii) Cell death was primarily caused by the rupture of the cell membrane when it reached a failure strain due to stresses exceeding critical threshold values. The loading and sliding at the cell–probe interface were key factors determining the pressure and shear stresses acting on the cell membrane. When the probe was in contact with cells, the pressure, shear stress, or a combination of both surpassed measurable critical thresholds, causing cell membrane rupture and subsequent cell death. These threshold values, measurable using advanced techniques, highlight the operation of mechanical stresses in tissue damage. Further studies on the micromechanical properties of cells, including their viscoelastic behaviour, are needed to fully understand how cells respond under different loading conditions.

(iii) Cell detachment was attributed to the dissociation of fibronectin fibrillar bonds at the cell–fibronectin junctions. Shear forces at the cell–probe interface were transmitted to the cell–fibronectin interface, resulting in the breaking of these adhesive bonds. A clear distinction was observed in the extent of cell detachment in the absence versus presence of a mucous boundary layer. Mucous boundary layers formed a hydrated barrier at the cell–probe interface, replacing the adhesive bonds typically formed during the cell–probe contact. This reduced the coefficient of friction and diminished the shear forces transmitted to the cell–fibronectin junctions, ultimately leading to fewer cell detachments.

The findings from this study provide a better understanding of interface-level mechanisms relevant to the development of alternative plant proteins. When coupled with sensory perception research, this approach offers a promising objective complement to traditional panel tests, helping reduce the subjectivity of sensory evaluations. Nevertheless, several challenges must still be addressed to bridge the gap between objective measurements and subjective sensory assessments of food. These include further investigation of interfacial phenomena such as the complexation of the mucous layer with astringent plant proteins, characterizing the micromechanical properties of the cell layer, as well as expanding studies to incorporate a wider range of food formulations.

Appendix Dynamic light scattering measurements

Particle sizes of 0.05% w/v purified BSM, 0.1% w/v FBPI, and 1:1 mixtures of 0.1% w/v FBPI, and 0.05% w/v purified BSM were measured using a Zetasizer (Malvern Panalytical, UK). A detailed description of the measurement technique is provided in Ref. [46]. Prior to testing, sample solutions were centrifuged at 20,000*g* for 30 min and the supernatant was collected for analysis. All DLS measurements were done at 32 angles at 25 °C.

The DLS results shown in Fig. A1 reveal two distinct size fractions for each protein investigated, as well as their mixture. BSM exhibited a major fraction with hydrodynamic diameters ranging from 60 to 460 nm (peak at 80 nm) and a smaller fraction ranging from 6 to 26 nm (peak at 11 nm). The FBPI dispersion displayed a larger fraction between 30 and 385 nm (peak at 46 nm) and a smaller fraction between 3 and 26 nm (peak at 8 nm). For experiments with the FBPI–BSM mixture, the smaller fraction ranged between 4 and 27 nm (peak at 14 nm), while the larger fraction was between 30 and 309 nm (peak at 59 nm).

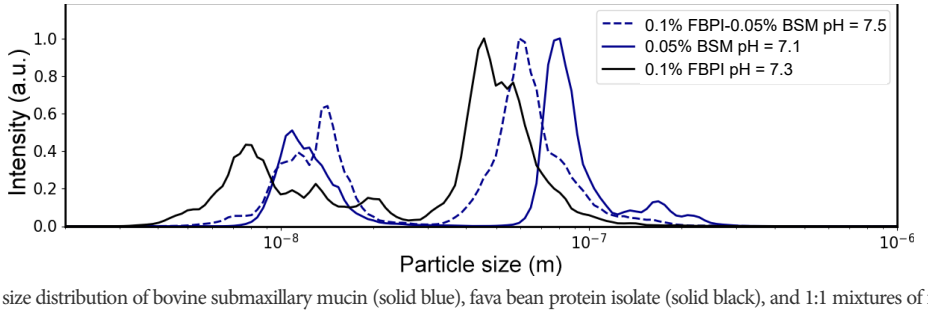


Fig. A1 Hydrodynamic size distribution of bovine submaxillary mucin (solid blue), fava bean protein isolate (solid black), and 1:1 mixtures of fava bean protein isolate and bovine submaxillary mucin (dashed blue) dispersions in PBS buffer solution.

Declaration of competing interest

The authors have no competing interests to declare that are relevant to the content of this article. The author Emile van der Heide is the Editorial Board member of this journal.

References

[1] Winkeljann B, Boettcher K, Balzer B N, Lieleg O. Mucin coatings prevent tissue damage at the cornea–contact lens interface. *Adv Materials Inter* **4**(19): 1700186 (2017)

[2] Wagner R, Carré M J, Perrault C M, Evans P C, Lewis R. Assessing friction and damage of cell monolayers on soft substrates in vitro. *J R Soc Interface* **21**(215): 20230696 (2024)

[3] Dunn A C, Zaveri T D, Keselowsky B G, Sawyer W G. Macroscopic friction coefficient measurements on living endothelial cells. *Tribol Lett* **27**(2): 233–238 (2007)

[4] Pitenis A A, Urueña J M, Hart S M, O'Bryan C S, Marshall S L, Levings P P, Angelini T E, Sawyer W G. Friction-induced inflammation. *Tribol Lett* **66**(3): 81 (2018)

[5] Gamaniel S S, de Vries E G, Tromp R H, de Hoog E H A, Vreeker R,

Matthews D T A, van der Heide E. Influence of plant-based compounds on the structural stability of mucous boundary layers in tribological contact. *Tribol Int* **209**: 110688 (2025)
[6] Holmberg K, Matthews A, Ronkainen H. Coatings tribology: Contact mechanisms and surface design. *Tribol Int* **31**(1–3): 107–120 (1998)
[7] Dwyer-Joyce R S. Predicting the abrasive wear of ball bearings by lubricant debris. *Wear* **233–235**: 692–701 (1999)
[8] Prakash S, Tan D D Y, Chen J S. Applications of tribology in studying food oral processing and texture perception. *Food Res Int* **54**(2): 1627–1635 (2013)
[9] Sharma M, Pondicherry K S, Duizer L. Understanding relations between rheology, tribology, and sensory perception of modified texture foods. *J Texture Stud* **53**(3): 327–344 (2022)
[10] Shewan H M, Pradal C, Stokes J R. Tribology and its growing use toward the study of food oral processing and sensory perception. *J Texture Stud* **51**(1): 7–22 (2020)
[11] Rudge R E D, Theunissen K, Stokes J R, Scholten E, Dijksman J A. Tribology of hard particles lubricating soft surfaces. *Phys Rev Materials* **5**(5): 055604 (2021)
[12] Kew B, Holmes M, Stieger M, Sarkar A. Oral tribology, adsorption and rheology of alternative food proteins. *Food Hydrocoll* **116**: 106636 (2021)
[13] Dresselhuis D, Dehoog E, Cohenstuart M, Vanaken G. Application of oral tissue in tribological measurements in an emulsion perception context. *Food Hydrocoll* **22**(2): 323–335 (2008)
[14] Malone M E, Appelqvist I A M, Norton I T. Oral behaviour of food hydrocolloids and emulsions. Part 1. Lubrication and deposition considerations. *Food Hydrocoll* **17**(6): 763–773 (2003)
[15] Andablo-Reyes E, Bryant M, Neville A, Hyde P, Sarkar R, Francis M, Sarkar A. 3D biomimetic tongue-emulating surfaces for tribological applications. *ACS Appl Mater Interfaces* **12**(44): 49371–49385 (2020)
[16] Madsen J B, Sotres J, Pakkanen K I, Efler P, Svensson B, Abou Hachem M, Arnebrant T, Lee S. Structural and mechanical properties of thin films of bovine submaxillary mucin versus porcine gastric mucin on a hydrophobic surface in aqueous solutions. *Langmuir* **32**(38): 9687–9696 (2016)
[17] Vlădescu S C, Agurto M G, Myant C, Boehm M W, Baier S K, Yakubov G E, Carpenter G, Reddyhoff T. Protein-induced delubrication: How plant-based and dairy proteins affect mouthfeel. *Food Hydrocoll* **134**: 107975 (2023)
[18] Yakubov G E, McColl J, Bongaerts J H H, Ramsden J J. Viscous boundary lubrication of hydrophobic surfaces by mucin. *Langmuir* **25**(4): 2313–2321 (2009)
[19] Rudge R E D, Fuhrmann P L, Scheermeijer R, van der Zanden E M, Dijksman J A, Scholten E. A tribological approach to astringency perception and astringency prevention. *Food Hydrocoll* **121**: 106951 (2021)
[20] Gamaniel S S, Dueñas Robles P S, Tromp H, de Hoog E H A, de Beer S, van der Heide E. A tribo-chemical view on astringency of plant-based food substances. *Friction* **12**(7): 1392–1407 (2024)
[21] Hertz H. Über die Berührung fester elastischer Körper. *J Reine Angew Math* **92**: 156–171 (1881)
[22] Gamaniel S S. Tribo-mechanical stability of mucous boundary layers in biofidelic contacts. Ph.D. Thesis. Enschede (the Netherlands): University of Twente, 2025.
[23] Schindelin J, Arganda-Carreras I, Frise E, Kaynig V, Longair M, Pietzsch T, Preibisch S, Rueden C, Saalfeld S, Schmid B, et al. Fiji: An open-source platform for biological-image analysis. *Nat Methods* **9**(7): 676–682 (2012)
[24] Schneider C A, Rasband W S, Eliceiri K W. NIH Image to ImageJ: 25 years of image analysis. *Nat Methods* **9**(7): 671–675 (2012)
[25] Kruskal W H, Wallis W A. Use of ranks in one-criterion variance analysis. *J Am Stat Assoc* **47**(260): 583–621 (1952)
[26] Contributors S, Virtanen P, Gommers R, Oliphant T E, Haberland M, Reddy T, Cournapeau D, Burovski E, Peterson P, Weckesser W, et al. Author correction: SciPy 1.0: Fundamental algorithms for scientific computing in Python. *Nat Methods* **17**(3): 352 (2020)
[27] Terpilowski M. Scikit-posthocs: Pairwise multiple comparison tests in Python. *JOSS* **4**(36): 1169 (2019)
[28] Weisenhorn A L, Khorsandi M, Kasas S, Gotzos V, Butt H J. Deformation and height anomaly of soft surfaces studied with an AFM. *Nanotechnology* **4**(2): 106–113 (1993)
[29] Massey A, Stewart J, Smith C, Parvini C, McCormick M, Do K, Cartagena-Rivera A X. Mechanical properties of human tumour tissues and their implications for cancer development. *Nat Rev Phys* **6**(4): 269–282 (2024)
[30] Engler A J, Chan M, Boettiger D, Schwarzbauer J E. A novel mode of cell detachment from fibrillar fibronectin matrix under shear. *J Cell Sci* **122**(Pt 10): 1647–1653 (2009)
[31] Peeters E A G, Bouten C V C, Oomens C W J, Baaijens F P T. Monitoring the biomechanical response of individual cells under compression: A new compression device. *Med Biol Eng Comput* **41**(4): 498–503 (2003)
[32] Peeters E A G, Oomens C W J, Bouten C V C, Bader D L, Baaijens F P T. Mechanical and failure properties of single attached cells under compression. *J Biomech* **38**(8): 1685–1693 (2005)
[33] Ludwig A, Kretzmer G, Schügerl K. Determination of a "critical shear stress level" applied to adherent mammalian cells. *Enzyme Microb Technol* **14**(3): 209–213 (1992)
[34] Thoumine O, Ott A, Cardoso O, Meister J J. Microplates: A new tool for manipulation and mechanical perturbation of individual cells. *J Biochem Biophys Meth* **39**(1–2): 47–62 (1999)
[35] Ghaednia H, Jackson R L. The effect of nanoparticles on the real area of contact, friction, and wear. *J Tribol* **135**(4): 041603 (2013)
[36] Yakubov G E, Branfield T E, Bongaerts J H H, Stokes J R. Tribology of particle suspensions in rolling–sliding soft contacts. *Biotribology* **3**: 1–10 (2015)
[37] Ding Y, Xu G K, Wang G F. On the determination of elastic moduli of cells by AFM based indentation. *Sci Rep* **7**: 45575 (2017)
[38] Ladjal H, Hanus J L, Pillarisetti A, Keefer C, Ferreira A, Desai J P. Atomic force microscopy-based single-cell indentation: Experimentation and finite element simulation. In: Proceedings of the IEEE/RSJ International Conference on Intelligent Robots and Systems, St. Louis, MO, USA, 2009: 1326–1332.
[39] Hofmann G, Jubin P, Gerligand P, Gallois-Bernos A, Franklin S, Smulders N, Gerhardt L C, Valster S. In-vitro method for determining corneal tissue friction and damage due to contact lens sliding. *Biotribology* **5**: 23–30 (2016)
[40] Wei H X, Wang Z Y, Tu X H, Cheng X S, Li L N, Wang S B, Li C W. Does static friction information predict the onset of sliding for soft material. *Int J Solids Struct* **305**: 113087 (2024)
[41] Lyashenko I, Borysiuk V. Stick–slip motion in the contact between soft elastomer and spherical hard steel indenter: Model explanation of superplasticity mode in metal samples with grain boundary defects. *Procedia Struct Integr* **36**: 24–29 (2022)
[42] Poletto J C, Neis P D, Fauconnier D, Ramalho A, De Baets P, Ferreira N F. A systematic investigation of grooving and rolling abrasive mechanisms using surface topography. *Wear* **548–549**: 205389 (2024)
[43] Li Y L, Schreiber P, Schneider J, Greiner C. Tribological mechanisms of slurry abrasive wear. *Friction* **11**(6): 1079–1093 (2023)
[44] Wagner R. In vitro damage quantification of medical device material interaction with endothelial cells. Ph.D. Thesis. Sheffield (UK): University of Sheffield, 2022.
[45] Romeo M, Mohlenhoff B, Jennings M, Diem M. Infrared micro-spectroscopic studies of epithelial cells. *Biochim Biophys Acta BBA Biomembr* **1758**(7): 915–922 (2006)
[46] Lorber B, Fischer F, Bailly M, Roy H, Kern D. Protein analysis by dynamic light scattering: Methods and techniques for students. *Biochem Molecular Bio Educ* **40**(6): 372–382 (2012)



Samuel S. Gamaniel obtained his Ph.D. degree in mechanical engineering from the University of Twente, in 2025. He is currently working as a postdoctoral researcher within the Chair of Skin Tribology at the University of Twente. His research interests are on the contact of soft biological tissues, tribology of plant protein products, and fluid film lubrication.



Ahranee Canden-Eastwood obtained her Ph.D. degree in tissue engineering and regenerative medicine from the University of Leeds, in 2023. Her Ph.D. research in injectable hydrogels for treatment of ankle osteoarthritis introduced her to the field of tribology and led to her work within the Human Interactions Group (HIG) at the University of Sheffield.



Sam Davison obtained his Ph.D. degree in tribology from the University of Sheffield, in 2023. His Ph.D. research into the performance of biodegradable lubricants has led to him from traditional machine contacts to biological contacts where he currently works as a research associate in the Human Interactions Group (HIG) at the University of Sheffield. Primarily focusing on experiment-based research, his current interests include aqueous lubricant performance, the tribology of mouth feel, and bio-derived friction modifiers.



Rob Vreeker earned his Ph.D. degree in physical chemistry from the University of Amsterdam, in 1987. He currently works at Cosun RD&I, the Netherlands, focusing on the physical chemistry and techno-functional properties of plant-based ingredients, with a particular interest in plant proteins.



David T. A. Matthews received his Ph.D. degree in applied physics and mathematics from the University of Groningen, the Netherlands, in 2008. Following nine years in industry as a principal researcher at Tata Steel, he is now an associate professor in surface design and engineering at the University of Twente, the Netherlands. His research interests surround the design and manufacture of surfaces for a wide range of applications and environments.



Matt J. Carré obtained his Ph.D. degree from the University of Sheffield, in 2000. He is currently a professor of mechanical engineering at the same institution. His main research interests are in biotribology, skin and tissue biomechanics, and the physical interactions between humans and systems/devices/environments.



Roger Lewis obtained his Ph.D. degree from the University of Sheffield, in 2000. He is currently a professor of mechanical engineering at the same institution. His main research interests are in biotribology and tribology of the wheel/rail interface.



Emile van der Heide obtained his Ph.D. degree in mechanical engineering from the University of Twente, in 2002. He worked for the Dutch Organization for Applied Scientific Research TNO as researcher, programme leader, and senior scientist in tribology. Currently, he holds the positions of Chair of the Mechanics of Solids Surfaces and Systems (MS3) department and Chair of the Skin Tribology group at the University of Twente. His research areas cover skin friction fundamentals, sensing & control of friction in product-skin interactions and on bio inspired interfaces.